John R.Horsley, Jingxian Yu, Kate L.Wegener, Christian Hoppmann, Karola Rück-Braun, Andrew D.Abell

Photoswitchable peptide-based 'on-off' biosensor for electrochemical detection and control of protein-protein interactions

Biosensors and Bioelectronics, 2018; 118:188-194

Photoswitchable peptide-based 'on-off' biosensor for electrochemical detection and control of protein-protein interactions

John R. Horsley[a], Jingxian Yu[a,*], Kate L. Wegener[b], Christian Hoppmann[c, 1], Karola Rück-Braun[c] and Andrew D. Abell[a,*]

[a] ARC Centre of Excellence for Nanoscale BioPhotonics (CNBP),
Department of Chemistry, University of Adelaide, SA 5005, Australia
[b] School of Biological Sciences, University of Adelaide, SA 5005, Australia
[c] Institut für Chemie, Technische Universität Berlin, Strasse des 17. Juni 135, 10623 Berlin, Germany

Abstract

Neuronal nitric oxide synthase (nNOS) is an enzyme responsible for catalyzing the production of the crucial cellular signalling molecule, nitric oxide (NO), through its interaction with the PDZ domain of α-syntrophin protein. In this study, a novel light-driven photoswitchable peptide-based biosensor, modelled on the nNOS β-finger, is used to detect and control its interaction with α-syntrophin. An azobenzene photoswitch incorporated into the peptide backbone allows reversible switching between a *trans* photostationary state devoid of secondary structure, and a *cis* photostationary state possessing a well-defined antiparallel β-strand geometry, as revealed by molecular modelling. Electrochemical impedance spectroscopy (EIS) is used to successfully detect the interaction between the gold electrode bound peptide in its *cis* photostationary state and a wide range of concentrations of α-syntrophin protein, highlighting both the qualitative and quantitative properties of the sensor. Furthermore, EIS demonstrates that the probe in its random *trans* photostationary state does not bind to the target protein. The effectiveness of the biosensor is further endorsed by the high thermal stability of the photostationary state of the *cis*-isomer, and the ability to actively control biomolecular interactions using light. This approach allows detection and control of binding to yield a regenerable on-off biosensor.

Keywords: Electrochemical impedance spectroscopy, protein-protein interaction, neuronal nitric oxide synthase (nNOS), photoswitchable peptides, biosensors, secondary structure.

*Corresponding authors
E-mail addresses: andrew.abell@adelaide.edu.au; jingxian.yu@adelaide.edu.au.

[1] Present address: Takara Bio USA, Inc.,1290 Terra Bella Ave, Mountain View, CA 94043, USA

1. Introduction

The detection of protein-protein interactions and other biomolecular interactions is commonly carried out using optical based sensors such as fluorescent probes and FRET based sensors. These optical methods use fluorescence or chemiluminescence to detect the interaction of the probe with its biological target (Silva et al. 2018), however this process can be limited by photobleaching and interference from background autofluorescence (Nakamura 2016). Such probes also require labelling with a fluorophore for signal detection, which can significantly alter binding to the biological target (Daniels and Pourmand 2007; Hushegyi et al. 2015). New approaches for studying and exploiting protein-protein interactions are needed in order to address these shortcomings, while recognizing that these interactions are predominantly transient, temporary and reversible in nature. Label-free, affinity-based techniques based on electrochemical signals present as an attractive option to allow direct detection of real-time events (Silva et al. 2018) with high selectivity and sensitivity (Mannoor et al. 2010) and with potential for future use in point-of-care applications (Chaudhary et al. 2016; Kang et al. 2017). Among these, electrochemical impedance spectroscopy (EIS) has become a powerful and informative technique for studying biorecognition processes, for example in the detection of antibodies (Afkhami et al. 2017), antibiotics (Hassani et al. 2017) and pathogens (Hou et al. 2018). In this approach, the electrical impedance of the probe and that of the probe/biological target complex, is measured as a function of the frequency of an applied electrical current to enable detection of a particular interaction. Impedance is the measure of opposition to the flow of electrical current (AC) when an external voltage is applied, and it possesses both magnitude and phase (cf. resistance, which possesses only magnitude). Biomolecular interactions between the ligand-modified sensor and a protein of interest, can be precisely correlated to changes in the impedance spectrum, providing a basis for rapid, non-destructive, robust, low-cost, and low-limits of detection (LOD) of biomolecules (Dibao-Dina et al. 2015; Fusco et al. 2017; Lim et al. 2017). Importantly, electrochemical transduction circumvents the need for labelling in optical-based methods, affording real-time measurement of the interaction while using less time and reagents than label-based methods (Templier et al. 2016), thus making EIS an ideal candidate for protein detection (Daniels and Pourmand 2007).

Here, we present an EIS-based probe that allows detection of α-1-syntrophin protein binding to a gold electrode bound azobenzene-containing peptide (**1**), derived from the β-finger of neuronal nitric oxide synthase (nNOS). Peptide **1** represents a truncated form of the native β-finger peptide that is known to bind to α-1-syntrophin *via* a well-defined protein-protein interaction. The azobenzene component allows reversible switching between a *trans* photostationary state (PSS) possessing an ill-defined conformation, and a *cis* PSS containing a well-defined secondary structure (see Figure 1) that mimics the bound form of the native nNOS β-finger ligand (Hoppmann et al. 2009). This photoswitching occurs with high spatiotemporal precision (Kumeria et al. 2015; Mourot et al. 2017). Attachment of **1** to a gold electrode (see Scheme 1) then allows detection of its interaction with the α-syntrophin protein by way of electrochemical impedance spectroscopy.

Neuronal nitric oxide synthase (nNOS) was chosen for this study because of its well-defined interaction with α-syntrophin protein and its important role in catalyzing the production of the crucial cellular signalling molecule nitric oxide (NO) (Nichols et al. 2015). We know that the β-finger ligand from the PDZ domain of nNOS forms an extended antiparallel β-sheet which interacts with the binding groove on the α-syntrophin PDZ domain to form a heterodimer (Hillier et al. 1999). PDZ protein interaction domains are among the most common protein modules, and in recent years have emerged as novel drug targets for disease (Pedersen et al. 2016), thus highlighting their potential in the development of tailored interfaces at the nanoscale.

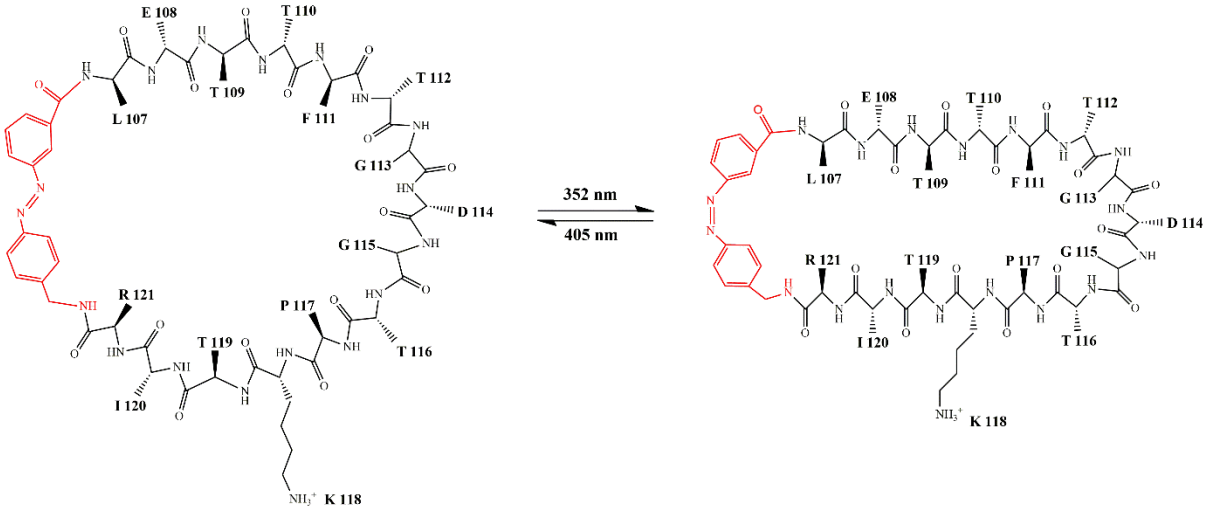

Figure 1. Schematic representation of photoswitchable cyclic peptide **1** with residues L107 to R121 retained from the native nNOS β-finger sequence. left: *trans* conformation, and right: *cis* conformation. The azobenzene photoswitch is highlighted in red.

2. Experimental

2.1 Electrode modification

The stepwise modification of gold electrodes is outlined in Scheme 1. Specifically, gold disk electrodes (Φ=2 mm) were polished with Metadi diamond pastes of 1 μm, and 0.25 μm particle sizes, and cleaned with sonication in Milli-Q water for 2 min. The polished electrodes were chemically treated in 25 % v/v H_2O_2 / KOH (50 mM) for 10 min, and then electrochemically cleaned by potential cycling between -400 mV and 1400 mV (vs. Ag/AgCl, 100 mV s^{-1}) for 50 cycles in 1.0 mM aqueous $HClO_4$ (Johari-Ahar et al. 2015). The electrodes were further subjected to potential cycling (step 1) between -200 mV and -1200 mV (vs. Ag/AgCl, 50 mV s^{-1}) for 50 cycles in 50 mM KOH (Kitagawa et al. 2008). The cleaned electrodes were immediately immersed in a 20 mM solution of 3-mercaptopropionic acid (MPA) in absolute ethanol at room temperature in the dark overnight, resulting in exposed carboxylic acid groups (step 2). Peptide **1** was then coupled to the electrode according to literature methodology. (Hoppmann et al. 2009). After the surface groups were activated to *N*-hydroxysuccinimide esters by NHS (0.05 M) / EDC (0.2 M) in HEPES buffer (50 mM, pH=8.5) for 30 min, the electrodes were exposed to a solution of peptide **1** (Hoppmann et al. 2011;

Hoppmann et al. 2009). Peptide **1** (0.1 mg ml^{-1}) was dissolved in the HEPES buffer containing NaCl (150 mM), and stirred at room temperature for 30 min, (step 3) allowing for binding of the lysine side chain of **1** (K118) to the modified electrode surface. Following the peptide immobilization reaction, the electrode was washed with methanol and blow-dried under N_2 flow. Photochemical induced isomerism of peptide **1** in HEPES buffer, from the *trans* to *cis* conformation as shown in Figure 1, was performed by irradiation with UV light (UVP MRL-58 lamp, 352 nm). Isomerism from *cis* to *trans* was carried out using visible light (Thorlabs LDC 201C Laser Diode Controller, LED 405 nm) (Freyer et al. 2009; Pearson and Abell 2010).

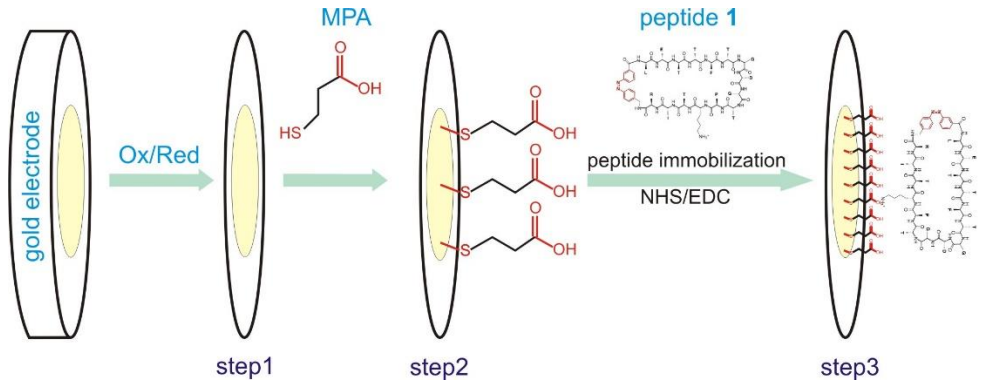

Scheme 1. Schematic representation of stepwise fabrication of electrochemical biosensor.

2.2 Preparation of α-syntrophin PDZ protein

The pET32a plasmid containing the mouse α-syntrophin PDZ domain sequence as a thioredoxin (TRX) fusion protein, with a centrally located His-tag, was expressed and purified as in (Seedorff et al. 2010). Briefly, the plasmid was transformed into BL21 (DE3) cells, which were grown to OD 0.8 in LB at 37°C, before induction with 0.1 mM IPTG and transferred to 30°C for 3.5 h. The culture was centrifuged and the cell pellet lysed by repetitive freeze-thawing, before further centrifugation. The clarified lysate was applied to a Ni-NTA column (BioRad) washed, and eluted with increasing concentrations of imidazole. Eluted fractions were combined and buffer exchanged using a PD10 desalting column (GE Healthcare) to remove imidazole, before treatment with enterokinase (Genscript, 50 units/10mg purified protein) at 20°C for 20 h. The His-tagged TRX domain and enterokinase were removed by reapplication to the Ni-NTA column. Purified PDZ domain was concentrated and lyophilized for storage. Immediately prior to the electrochemical experiments, the domain was resuspended and exchanged into 50 mM HEPES (pH=8.5) and 150 mM NaCl, at a final concentration of 230 μM, based on an extinction coefficient of 2980 M^{-1} cm^{-1} (λ=280 nm).

2.3 Electrochemical measurements

All electrochemical measurements were carried out in a conventional three-electrode electrochemical cell at room temperature, using an Autolab PGSTAT204 analyser (Metrohm Autolab, B.V.) equipped with an FRA32M electrochemical impedance spectroscopy module. The peptide **1**-modified electrode formed the working electrode, with a platinum mesh and Ag/AgCl wire used as the respective counter and reference electrodes. Both cyclic voltammetric and impedance measurements were performed to monitor the stepwise modification of gold electrodes, in 50 mM HEPES, 150 mM NaCl solution (pH=7.5) and 2

mM $K_4Fe(CN)_6$ as a redox probe. All solutions were prepared with analytical grade reagents in Milli Q water, purged with nitrogen gas. The interaction of the α-syntrophin PDZ domain protein with surface-bound peptide **1** was conducted at various concentrations (3.25 μM, 7.80 μM, 22.45 μM and 40.25 μM), using an electrochemical impedance technique in 2 mM $K_4Fe(CN)_6$, 50 mM HEPES and 150 mM NaCl (pH=7.5) buffer solution. Electrochemical impedance measurements were undertaken in the frequency range 10^{-1} Hz to 10^5 Hz at the formal potential of 220 mV *vs* Ag/AgCl with an AC amplitude of ±10 mV. All impedance data were fitted to the proposed equivalent circuit using the EvolCRT program (Yu et al. 2007).

2.4 Molecular modelling

Initial *cis* and *trans* geometries of cyclic peptide **1** were prepared using the GaussView 5.0 package by modifying the corresponding β-finger of the extended nNOS PDZ domain (crystal structure code 1QAU) (Hillier et al. 1999), with an azobenzene moiety (as shown in Figure 1, highlighted in red). The lowest energy conformers were determined in the gas phase using the NWChem 6.6 package (Valiev et al. 2010), with tight convergence criteria using a hybrid B3LYP method with 6-31G** basis set for all atoms, in order to define the backbone conformations. Conformational analysis, including dihedral angles, overall molecular lengths and intramolecular hydrogen bond lengths, was conducted using the Chimera 1.11 package (Pettersen et al. 2004).

3. Results and discussion

3.1 Design of electrochemical peptide-based sensor for biomolecular interactions

PDZ domains, such as those in nNOS and α-1-syntrophin, interact with β-strand motifs at a groove formed by α-helix-1 and the β-sheet. PDZ binding motifs are typically found in linear C-terminal protein extensions, but can also be found internally, such as in the nNOS PDZ domain. This protein contains a 30 residue β-hairpin region, otherwise known as the β-finger, which is required for the formation of the heterodimer complex with α-1-syntrophin, docking into the carboxyl peptide binding groove of the α-syntrophin PDZ domain (Tochio et al. 2000). Peptide **1** is designed to mimic the β-finger of nNOS with residues L107 through R121 retained from the native protein (see Figure 1). The azobenzene component links the *N*-terminus of L107 to the C-terminus of R121 to provide a macrocycle, the conformation of which is then modulated by photochemical induced isomerism. Peptide **1** is covalently attached to the NHS-activated gold working electrode by coupling to the primary amine of lysine residue K118, as illustrated in Scheme 1. Cyclic voltammetry and EIS are used to characterize each step of the electrode interfacial modifications, and detection of the interaction between peptide **1** and the α-syntrophin protein is revealed through EIS.

3.2 Electrochemical characterization of the stepwise-modified electrodes

Cyclic voltammetry shows a well-defined, reversible redox wave of ferricyanide ions for the bare gold electrode (Figure 2a, red curve, step 1) with a peak-to-peak separation (ΔE_p) of 69 mV at a scan rate of 100 mV s^{-1}. Following the immobilization of mercaptopropionic acid

(MPA) linkers (green curve, step 2), the amperometric response of the redox couple decreases, with an increase in the peak-to-peak separation. Clearly, immobilization of the MPA linker induces an additional electron transfer barrier between the redox species in solution and the gold surface. Next, peptide **1** (*trans* PSS) is covalently attached to the exposed carboxylic acid groups on the surface *via* the lysine residue (K118) on the underside strand (Figure 2a, step 3-*trans*). The *cis* PSS of peptide **1** is obtained on irradiation of UV light (352 nm), with the associated voltammogram (black curve) showing a decrease in the amperometric response from step 2, accompanied by an increase in peak-to-peak separation. In contrast, immobilization of the *trans* PSS of **1** gives rise to a notable increase in the amperometric response (blue curve). The voltammetric disparity between both photostationary states of **1** attached to the electrode surface, suggests that the *cis* PSS forms a more densely packed monolayer, while immobilization of the *trans* PSS very likely distorts the homogeneity of the MPA monolayer (step 2).

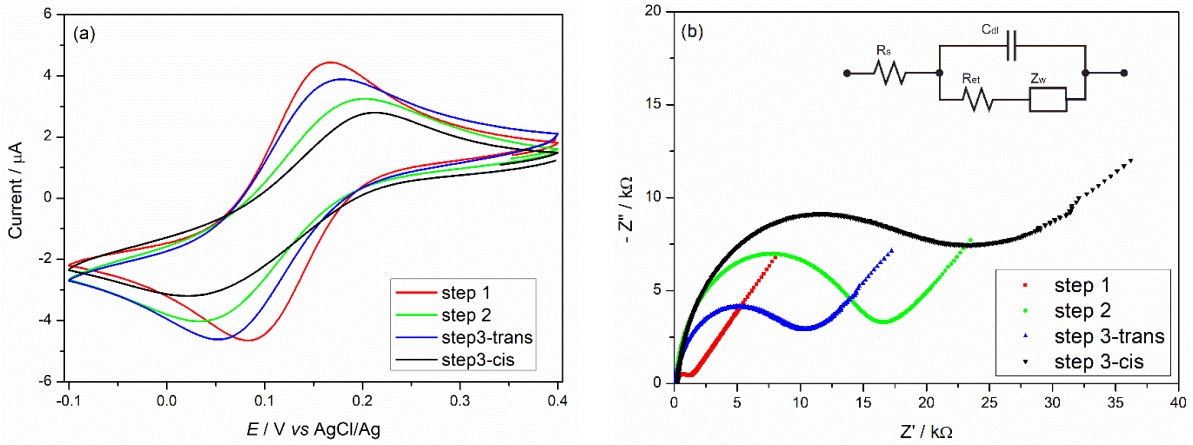

Figure 2. (a) Cyclic voltammograms and (b) Nyquist impedance plots of the stepwise-modified gold electrodes in 2 mM $K_4Fe(CN)_6$, 50 mM HEPES and 150 mM NaCl (pH=7.5) buffer solution. The inset in (b) shows the equivalent circuit model used for impedance data analysis. Step 1 represents the cyclic voltammogram and Nyquist plot for the cleaned bare gold electrode (red), step 2 with mercaptopropionic acid (MPA) linkers (green), step 3-*trans* with surface-bound *trans* PSS of peptide **1** (blue), and step 3-*cis* with surface-bound *cis* PSS of peptide **1** (black).

The interfacial charge transfer properties of each modification step were also monitored by electrochemical impedance spectroscopy (EIS). The corresponding complex plane impedance plots are presented in Figure 2b, each of which comprises one semicircle in high frequency range and a straight line in low frequency range. The semicircle reflects the electron transfer kinetics of the $Fe(CN)_6^{3-/4-}$ redox pair at the electrode surface, while the straight line indicates diffusion of the redox from the solution to the surface (Cai et al. 2017) (Chen et al. 2018). The equivalent circuit model shown in Figure 2b (inset) was adopted for the impedance data analysis and contains four electrical elements, namely, the electrolyte resistance (R_s), double-layer capacitance (C_{dl}), charge transfer resistance (R_{et}) and the Warburg element (Z_w). Here, the diameter of the respective semicircles shown in Figure 2b directly corresponds to the charge transfer resistance (R_{et}) of each modification step. As expected, the R_{et} value for the bare gold electrode (red curve) is the lowest (936 Ω), reflecting its high conductibility. Following immobilization of the MPA linker (green curve) onto the electrode surface, the R_{et} value

increases to 14274 Ω, indicating the introduction of an additional electron transfer barrier. The R_{et} value for peptide **1** (*trans* PSS) was observed to be 8569 Ω, however when the peptide is irradiated to the *cis* configuration using UV light (352 nm), the R_{et} value increases dramatically to 19374 Ω (see Figure 2b). The EIS results correlate well with the cyclic voltammetric data, with both techniques establishing a clear and measurable distinction between the structural/electronic properties of the two photostationary states. A detailed conformational analysis of both isomers of peptide **1** was conducted to define precise structural differences and hence shed further light on their interaction with the target protein.

3.3 Computational conformational comparison of *cis* and *trans* isomers of peptide **1**

Lowest energy conformers and hence backbone geometries, of the *cis* and *trans* isomers of peptide **1** were determined by the density functional theory (DFT) method (see Figure 3). The models for both isomers reveal much detail on the secondary structure crucial for binding to the PDZ domain of α-syntrophin protein. The rigid conformation of the β-finger in the intact nNOS PDZ domain is stabilized by a salt bridge linking the β-finger (R121) to the main body of the PDZ domain (D 62) (Hillier et al. 1999). Here, the β-hairpin structure (peptide **1**) is stabilized by the *cis* azobenzene photoswitch bringing the two β-strands into close proximity as shown in Figure 3a. The *cis* isomer of peptide **1** adopts an antiparallel β-sheet, with the dihedral angles of residues L107 – T112, and T116 – R121 consistent with a β-strand structure (Horsley et al. 2015; Horsley et al. 2014) (see Table S1). A total of eight strong intramolecular backbone hydrogen bonds link the two strands of the *cis* isomer of **1** to form the β-sheet (see Figure 3a and Table S3). Intramolecular hydrogen bonds of less than 2 Å in length are apparent between the backbones of E108/I120, T110/K118 and T112/T116, which are consistent with a previous NMR study on a biosynthetic peptide derived from the native nNOS β-finger (Wang et al. 2000). Furthermore, a strong hydrogen bond is evident between the CO of T112 (*i*) and the NH of G115 (*i*+3), together with a distance of less than 7 Å between the Cα atoms of residues *i* and *i*+3 (5.7 Å, see Figure S5), both prerequisites for a valid β-turn (Chou 2000). Interestingly, the dihedral angles of the threonine residue (T112) located in the (*i*) position of the turn are consistent with a β-strand, indicating the presence of this secondary structure throughout the hairpin, with the two flexible glycines of the β-turn (G113, G115) flanking the D114 (*i*+2) residue. Collectively, this data reveals a 'class 3 three-residue β-hairpin' structure within the *cis* isomer of peptide **1** (Milner-White and Poet 1986). In contrast, the *trans* photoswitch is extended to such an extent (11 Å, see Figure S2) as to disrupt all intramolecular hydrogen bonding, resulting in a distorted peptide with a random structure (see Figure 3b, Table S2). The overall lengths of the peptides differ greatly, with the *cis* isomer measuring 29 Å, and the *trans* isomer 17 Å (see Table S3, Figures S3, S4). This high-level computational study confirms the conformation of the *trans* isomer to be ill-defined, and demonstrates the propensity of the azobenzene photoswitch to maintain a stable antiparallel β-sheet structure when peptide **1** is in the *cis* configuration.

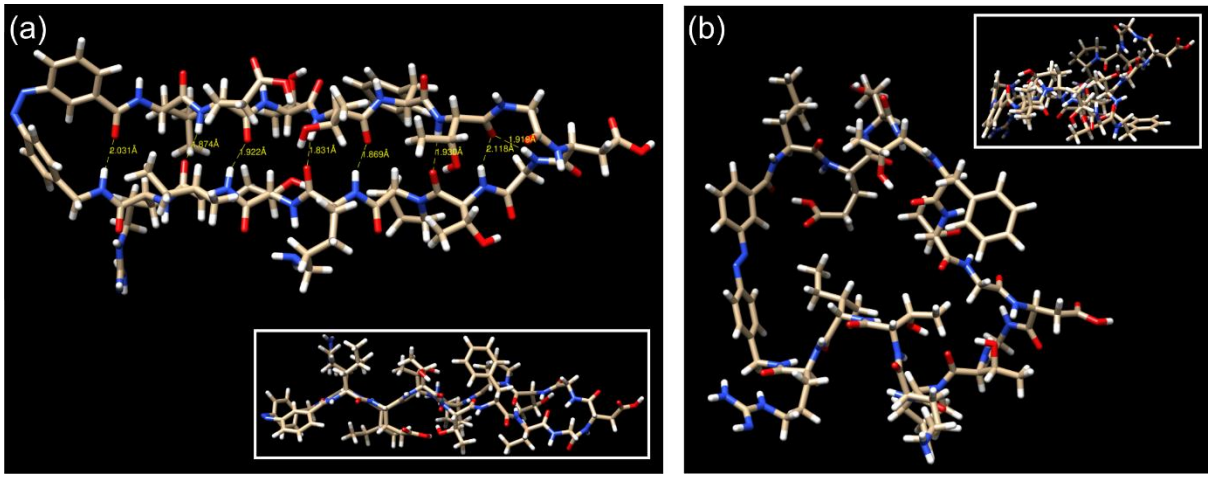

Figure 3. Molecular model representative of peptide **1** in (a) *cis* conformation, showing intramolecular hydrogen bonding, and (b) *trans* conformation, using a hybrid B3LYP functional with 6-31G** basis set for all atoms. (Insets for both peptides: top view looking down).

3.4 Detection of binding between surface-bound peptide **1** and α-syntrophin PDZ domain

The EIS probe, with peptide **1** in its well-defined *cis* PSS, was then exposed to a solution of α-syntrophin PDZ domain protein (7.80 μM) in HEPES buffer (pH 7.5). A 95% increase in the R_{et} value is observed, from 19374 Ω prior to incubation, to 37780 Ω following incubation (see Figure 4a). This significant gain clearly confirms the ability of the probe to detect and measure the biomolecular interaction between the peptide and the specific protein target. Peptide **1** was then irradiated at 405 nm for conversion to the *trans* PSS, and introduced to a solution of the target protein. As such, the protein is not exposed to irradiation. The observed R_{et} value for the *trans* PSS in the presence of α-syntrophin PDZ domain (7.80 μM) is 9245 Ω, compared to 8569 Ω prior to incubation (see Figure 4b). As the absorption spectra of *cis* and *trans* photostationary states of azobenzene overlap, the maximum attainable *trans* PSS is approximately 95% (Beharry and Woolley 2011). This minimal increase observed in the charge transfer resistance (7%) is consistent with having attained maximum *trans* PSS with minimal *cis* isomer content. Thus, the *trans* PSS with its random, ill-defined structure is clearly not binding to α-syntrophin. These experimental electrochemical impedance results are consistent with observations from a previous *in vitro* SPR-based study (Hoppmann et al. 2009) thus highlighting the synergy between these two sensing platforms. This study observed a maximum achievable *cis* content of 90%, and found the *cis* PSS of peptide **1** to possess high thermal stability and robustness, a prerequisite for a functional biosensor.

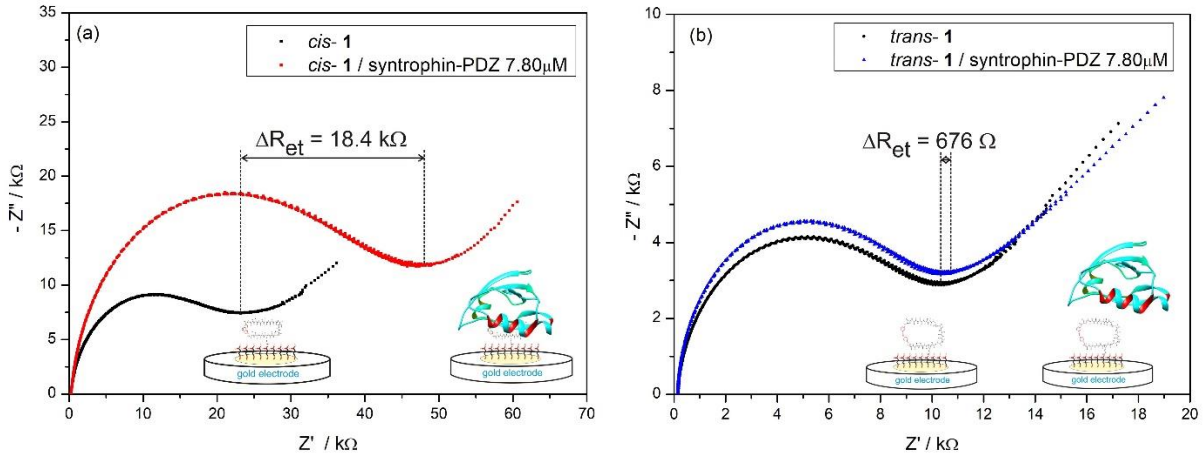

Figure 4. Nyquist plots for surface-bound (a) *cis* PSS and (b) *trans* PSS of peptide **1** in the presence of α-syntrophin PDZ domain (7.80 μM), plus 2 mM $K_4Fe(CN)_6$, 50 mM HEPES and 150 mM NaCl (pH=7.5). [Schematic representation demonstrates binding of *cis* PSS of the peptide **1**-modified electrode to α-syntrophin protein (left), whereas *trans* PSS does not bind (right)].

The *cis* PSS of the peptide **1**-modified electrode was then exposed to various concentrations of the target protein, ranging from 3.25 μM to 40.25 μM. Three electrodes were tested at each concentration. As the concentration of α-syntrophin increases incrementally, so too does the charge transfer resistance, confirming both the qualitative and quantitative properties of the biosensor (see Figure 5a). The experimental results further reveal that the relative standard deviations (RSD) range from 1.01% to 1.64% for the above-mentioned concentrations, indicating good reproducibility of the biosensor. Saturation is reached at a concentration of approximately 40 μM with the R_{et} value peaking at 42259 ± 426 Ω (see Figure 5b). Thus a total increase of over 100% in the charge transfer resistance (R_{et}) was achieved from the isolated probe in its *cis* PSS (Figure 5a, black line), further demonstrating the efficacy of the biosensor.

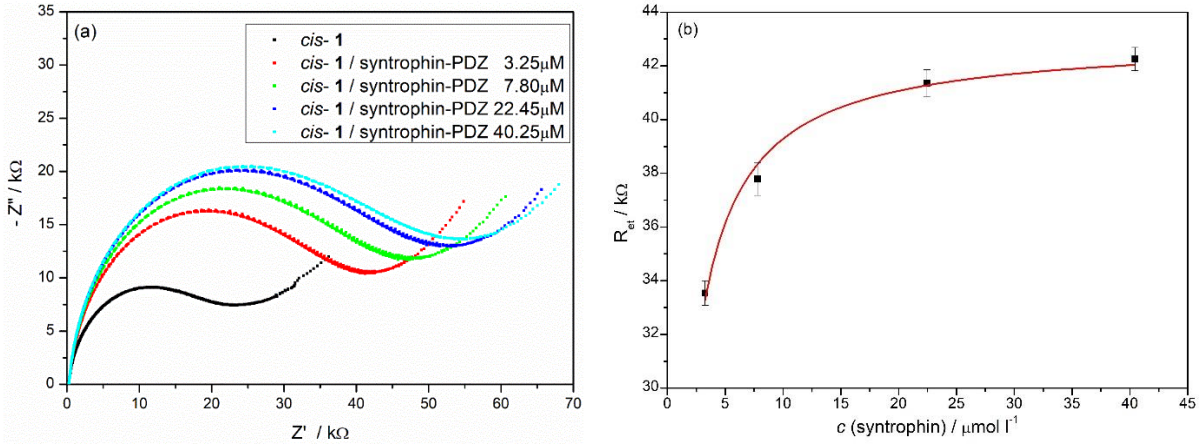

Figure 5. (a) Nyquist plots for the *cis*-PSS of **1** bound to the PDZ domain of α-syntrophin at concentrations ranging from 3.25 μM to 40.25 μM. (b) Dependence of charge transfer resistance (R_{et}) on the concentration of α-syntrophin PDZ domain.

4. Conclusions

Advancing our awareness and understanding of protein-protein interaction affinity and associated biological activity is crucial to progress the next generation of technology, such as implantable biosensors for medical applications and light-activated drug delivery. Here, we have successfully developed a photoswitchable peptide-based biosensor for the detection of protein-protein interactions using electrochemical impedance spectroscopy (EIS). The peptide is derived from the β-finger region of neuronal nitric oxide synthase (nNOS), which is essential for the catalysis of nitric oxide (NO) through its interaction with the PDZ domain of α-1-syntrophin protein. The incorporation of an azobenzene photoswitch into peptide **1** allows photochemical control of the geometry, enabling switching between a random structure (*trans* isomer), and one with a well-defined β-strand secondary structure (*cis* isomer) that mimics that of the native nNOS β-finger ligand to facilitate binding to α-1-syntrophin. The observed electrochemical data clearly demonstrates that the *cis* PSS of the peptide **1**-modified probe binds to the PDZ domain of α-1-syntrophin protein, whereas the corresponding ill-defined *trans* PSS does not. This is the first demonstration of a simultaneous evaluation of electrochemical impedance responses from an EIS biosensor in reference to *cis* and *trans* photostationary states of a peptide. This approach should be generally applicable to studying a range of protein-protein interactions where surface domains exist to facilitate binding and these usually contain an element of well-defined secondary structure, such as β-strands and/or helices that can be incorporated into a probe to facilitate molecular interaction. Moreover, the strategy outlined here provides an opportunity to turn the probe on and off to allow on-demand detection, facilitating active control over biomolecular interactions.

Acknowledgements

The authors acknowledge funding from the Centre for Nanoscale BioPhotonics (CNBP), through the Australian Research Council (ARC) CE140100003, and the National Health and Medical Research Council (NHMRC) APP1068087. We thank Dr Anne Diehl and Dr Peter Schmieder, Leibniz Institute for Molecular Pharmacology, Berlin, for providing the plasmid containing the α-syntrophin PDZ domain sequence. The computational aspects of this work were supported by an award under the National Computational Merit Allocation Scheme (NCMAS) Y84, for JY through the National Computing Infrastructure (NCI) National Facility at the Australian National University.

Declarations of interest: none

Supplementary material

5. References

Afkhami, A., Hashemi, P., Bagheri, H., Salimian, J., Ahmadi, A., Madrakian, T., 2017. Impedimetric immunosensor for the label-free and direct detection of botulinum neurotoxin serotype A using Au nanoparticles/graphene-chitosan composite. Biosensors and Bioelectronics 93(Supplement C), 124-131.
Beharry, A.A., Woolley, G.A., 2011. Azobenzene photoswitches for biomolecules. Chemical Society Reviews 40(8), 4422.
Cai, W., Xie, S., Zhang, J., Tang, D., Tang, Y., 2017. An electrochemical impedance biosensor for Hg2+ detection based on DNA hydrogel by coupling with DNAzyme-assisted target recycling and hybridization chain reaction. Biosensors and Bioelectronics 98(Supplement C), 466-472.
Chaudhary, P.M., Gade, M., Yellin, R.A., Sangabathuni, S., Kikkeri, R., 2016. Targeting label free carbohydrate-protein interactions for biosensor design. Analytical Methods 8(17), 3410-3418.
Chen, S., Liu, P., Su, K., Li, X., Qin, Z., Xu, W., Chen, J., Li, C., Qiu, J., 2018. Electrochemical aptasensor for thrombin using co-catalysis of hemin/G-quadruplex DNAzyme and octahedral Cu2O-Au nanocomposites for signal amplification. Biosensors and Bioelectronics 99(Supplement C), 338-345.
Chou, K.-C., 2000. Prediction of Tight Turns and Their Types in Proteins. Analytical Biochemistry 286(1), 1-16.
Daniels, J.S., Pourmand, N., 2007. Label-Free Impedance Biosensors: Opportunities and Challenges. Electroanalysis 19(12), 1239-1257.
Dibao-Dina, A., Follet, J., Ibrahim, M., Vlandas, A., Senez, V., 2015. Electrical impedance sensor for quantitative monitoring of infection processes on HCT-8 cells by the waterborne parasite Cryptosporidium. Biosensors and Bioelectronics 66(Supplement C), 69-76.
Freyer, W., Brete, D., Schmidt, R., Gahl, C., Carley, R., Weinelt, M., 2009. Switching behavior and optical absorbance of azobenzene-functionalized alkanethiols in different environments. Journal of Photochemistry and Photobiology A: Chemistry 204(2), 102-109.
Fusco, G., Gallo, F., Tortolini, C., Bollella, P., Ietto, F., De Mico, A., D'Annibale, A., Antiochia, R., Favero, G., Mazzei, F., 2017. AuNPs-functionalized PANABA-MWCNTs nanocomposite-based impedimetric immunosensor for 2,4-dichlorophenoxy acetic acid detection. Biosensors and Bioelectronics 93(Supplement C), 52-56.
Hassani, N.E.A.E., Baraket, A., Neto, E.T.T., Lee, M., Salvador, J.P., Marco, M.p., Bausells, J., Bari, N.E., Bouchikhi, B., Elaissari, A., Errachid, A., Zine, N., 2017. Novel strategy for sulfapyridine detection using a fully integrated electrochemical Bio-MEMS: Application to honey analysis. Biosensors and Bioelectronics 93, 282-288.
Hillier, B.J., Christopherson, K.S., Prehoda, K.E., Bredt, D.S., Lim, W.A., 1999. Unexpected Modes of PDZ Domain Scaffolding Revealed by Structure of nNOS-Syntrophin Complex. Science 284(5415), 812-815.
Hoppmann, C., Schmieder, P., Domaing, P., Vogelreiter, G., Eichhorst, J., Wiesner, B., Morano, I., Rück-Braun, K., Beyermann, M., 2011. Photocontrol of Contracting Muscle Fibers. Angewandte Chemie International Edition 50(33), 7699-7702.
Hoppmann, C., Seedorff, S., Richter, A., Fabian, H., Schmieder, P., Rueck-Braun, K., Beyermann, M., 2009. Light-Directed Protein Binding of a Biologically Relevant beta-Sheet. Angewandte Chemie-International Edition 48(36), 6636-6639.
Horsley, J.R., Yu, J., Abell, A.D., 2015. The Correlation of Electrochemical Measurements and Molecular Junction Conductance Simulations in β-Strand Peptides. Chemistry A European Journal 21, 5926-5933.
Horsley, J.R., Yu, J., Moore, K.E., Shapter, J.G., Abell, A.D., 2014. Unraveling the Interplay of Backbone Rigidity and Electron Rich Side-Chains on Electron Transfer in Peptides: The Realization of Tunable Molecular Wires. Journal of the American Chemical Society 136, 12479-12488.
Hou, Y.-H., Wang, J.-J., Jiang, Y.-Z., Lv, C., Xia, L., Hong, S.-L., Lin, M., Lin, Y., Zhang, Z.-L., Pang, D.-W., 2018. A colorimetric and electrochemical immunosensor for point-of-care detection of enterovirus 71. Biosensors and Bioelectronics 99, 186-192.

Hushegyi, A., Bertok, T., Damborsky, P., Katrlik, J., Tkac, J., 2015. An ultrasensitive impedimetric glycan biosensor with controlled glycan density for detection of lectins and influenza hemagglutinins. Chemical Communications 51(35), 7474-7477.
Johari-Ahar, M., Rashidi, M.R., Barar, J., Aghaie, M., Mohammadnejad, D., Ramazani, A., Karami, P., Coukos, G., Omidi, Y., 2015. An ultra-sensitive impedimetric immunosensor for detection of the serum oncomarker CA-125 in ovarian cancer patients. Nanoscale 7(8), 3768-3779.
Kang, D., Sun, S., Kurnik, M., Morales, D., Dahlquist, F.W., Plaxco, K.W., 2017. New Architecture for Reagentless, Protein-Based Electrochemical Biosensors. Journal of the American Chemical Society 139(35), 12113-12116.
Kitagawa, Y., Hobara, D., Yamamoto, M., Kakiuchi, T., 2008. Counterion binding induces attractive interactions between negatively-charged self-assembled monolayer of 3-mercaptopropionic acid on Au(111) in reductive desorption. Journal of Solid State Electrochemistry 12(4), 461-469.
Kumeria, T., Yu, J., Alsawat, M., Kurkuri, M.D., Santos, A., Abell, A.D., Losic, D., 2015. Photoswitchable Membranes Based on Peptide-Modified Nanoporous Anodic Alumina: Toward Smart Membranes for On-Demand Molecular Transport. Advanced Materials 27(19), 3019-3024.
Lim, J.M., Ryu, M.Y., Yun, J.W., Park, T.J., Park, J.P., 2017. Electrochemical peptide sensor for diagnosing adenoma-carcinoma transition in colon cancer. Biosensors and Bioelectronics 98(Supplement C), 330-337.
Mannoor, M.S., Zhang, S., Link, A.J., McAlpine, M.C., 2010. Electrical detection of pathogenic bacteria via immobilized antimicrobial peptides. Proceedings of the National Academy of Sciences 107(45), 19207-19212.
Milner-White, E.J., Poet, R., 1986. Four classes of β-hairpins in proteins. Biochemical Journal 240(1), 289-292.
Mourot, A., Herold, C., Kienzler, M.A., Kramer, R.H., 2017. Understanding and improving photo-control of ion channels in nociceptors with azobenzene photo-switches. British Journal of Pharmacology, 1-16.
Nakamura, Y.H., T. Nagaya, T. Sato, K. Okuyama, S. Choyke, P. Kobayashi, H., 2016. Dynamic fluorescent imaging with the activatable probe, γ-glutamyl hydroxymethyl rhodamine green in the detection of peritoneal cancer metastases. Oncotarget 7, 51124-51137.
Nichols, B., Takeda, S., Yokota, T., 2015. Nonmechanical Roles of Dystrophin and Associated Proteins in Exercise, Neuromuscular Junctions, and Brains. Brain Sciences 5(3), 275.
Pearson, D., Abell, A.D., 2010. Structural Optimization of Photoswitch Ligands for Surface Attachment of alpha-Chymotrypsin and Regulation of Its Surface Binding. Chemistry-a European Journal 16(23), 6983-6992.
Pedersen, S.W., Moran, G.E., Sereikaitė, V., Haugaard-Kedström, L.M., Strømgaard, K., 2016. Importance of a Conserved Lys/Arg Residue for Ligand/PDZ Domain Interactions as Examined by Protein Semisynthesis. ChemBioChem 17(20), 1936-1944.
Pettersen, E.F., Goddard, T.D., Huang, C.C., Couch, G.S., Greenblatt, D.M., Meng, E.C., Ferrin, T.E., 2004. UCSF Chimera—A visualization system for exploratory research and analysis. Journal of Computational Chemistry 25(13), 1605-1612.
Seedorff, S., Appelt, C., Beyermann, M., Schmieder, P., 2010. Design, synthesis, structure and binding properties of PDZ binding, cyclic β-finger peptides. Biochemical and Biophysical Research Communications 395(4), 535-539.
Silva, N.F.D., Magalhães, J.M.C.S., Freire, C., Delerue-Matos, C., 2018. Electrochemical biosensors for Salmonella: State of the art and challenges in food safety assessment. Biosensors and Bioelectronics 99(Supplement C), 667-682.
Templier, V., Roux, A., Roupioz, Y., Livache, T., 2016. Ligands for label-free detection of whole bacteria on biosensors: A review. TrAC Trends in Analytical Chemistry 79(Supplement C), 71-79.
Tochio, H., Mok, Y.-K., Zhang, Q., Kan, H.-M., Bredt, D.S., Zhang, M., 2000. Formation of nNOS/PSD-95 PDZ dimer requires a preformed β-finger structure from the nNOS PDZ domain11Edited by M. F. Summers. Journal of Molecular Biology 303(3), 359-370.

Valiev, M., Bylaska, E.J., Govind, N., Kowalski, K., Straatsma, T.P., van Dam, H.J.J., Wang, D., Nieplocha, J., Apra, E., Windus, T.L., de Jong, W.A., 2010. NWChem: a comprehensive and scalable open-source solution for large scale molecular simulations. Computer Physics Communications 181, 1477.
Wang, P., Zhang, Q., Tochio, H., Fan, J.-S., Zhang, M., 2000. Formation of a native-like β-hairpin finger structure of a peptide from the extended PDZ domain of neuronal nitric oxide synthase in aqueous solution. European Journal of Biochemistry 267(11), 3116-3122.
Yu, J., Cao, H., He, Y., 2007. A new tree structure code for equivalent circuit and evolutionary estimation of parameters. Chemometrics and Intelligent Laboratory Systems 85(1), 27-39.